Chapter 5

PWM Waveform Generation Using Pulse-Type Hardware Neural Networks

This chapter presents the pulse-type hardware neural networks (P-HNN) which could output the pulse width modulation (PWM) waveform of the PWM servo motor for robots. The basic component of the P-HNN is the pulse-type hardware neuron model (P-HNM). The P-HNM generates oscillatory patterns of electrical activity similar to those of living organisms. Basic components of the P-HNM consist of the cell body model, the axon model and the synaptic model. The P-HNM has the same basic features of biological neurons, such as threshold, refractory period and spatiotemporal summation characteristics, and enables the generation of continuous action potentials. In this chapter, we used the synaptic model which could vary the synaptic weights by controlling voltage. The P-HNN could output several pulse widths of the PWM waveform by varying the synaptic weights. As a result, we show that P-HNN could control the PWM servo motor from 0° to 180°. The P-HNN realized the control of the PWM servo motor without using any software programs, or A/D converters. In addition, it is shown that the pulse waveform generation method of the P-HNM is the same as for living organisms.

Chapter written by Ken SAITO, Minami TAKATO, Yoshifumi SEKINE and Fumio UCHIKOBA.

5.1. Introduction

The PWM controlling system was often used for several types of robot controlling systems. The PWM controlling system was easily controlled by the programmed control. Therefore, the programmed control by microcontroller has been the dominant system among robot controlling systems, such as locomotion controlling system or sensory information processing system [KAZ 98]. In the future, a robot controlling system will require an increasingly higher functionalization to play an important role in human living space. However, higher functionalization of a programmed control is difficult because the microcontroller has a limitation in memory capacity. Therefore, operational control by an operator was undertaken in complicated or unprogrammed situations. These robot controlling systems were not flexible autonomous controlling systems. On the other hand, neural networks (NN) of living organisms have excellent information processing functions for controlling systems [KIY 87, GEN 95, SIM 00, NAO 01, GIS 01]. This is because living organisms make excellent decisions to control locomotion according to the sensory information from external situations. For this reason, various studies are investigating the implementation of neural computers using new algorithms based on the principles of living brains. In particular, oscillatory patterns of electrical activity are a ubiquitous feature in nervous systems. Living organisms use several oscillatory patterns for movement, swallowing, heart rhythms, etc. [DEL 80, MIC 02]. Coupled neural oscillators are drawing attention to clarify oscillatory patterns. Synchronization phenomena or bifurcation phenomena of coupled neural systems have been studied using the Hodgkin–Huxley model or the Bonhoeffer–van der Pol model, which is a mathematical class II neuron [KUN 03, KUN 06, SHI 07]. In addition, Fujitsu Automation developed the small humanoid robot: HOAP-1, HOAP-2 and HOAP-3, which can generate robotic motion using the mathematical neural network (NeuROMA) [JIA 02, RIA 02]. NeuROMA is based on the biological central pattern generator (CPG), which is a locomotion controller for living organisms.

Earlier, various supercomputers were constructed for developing the information processing capability to calculate the research which has large computational effort (http://www.top500.org/). Nevertheless, to simulate the excellent information processing functions of living organisms, the computational effort becomes great using, a high-nonlinearity neuron model. Therefore, the mathematical neuron model in large-scale NN is difficult to process in continuous time because the simulation is limited by

the computer's performance, such as the processing speed and the memory capacity. In contrast, hardware models are advantageous because, even if a circuit scale becomes large, a nonlinear operation can be processed at high speed. Therefore, the construction of a hardware model that can generate oscillatory patterns is desired because nonlinear operations can be processed at higher speeds than the mathematical model. The hardware ring coupled oscillators have already been studied as a system which can demonstrate the various oscillatory patterns and the synchronization phenomena [END 78, KIT 01]. For this reason, the ring coupled oscillators are expected to be a structural element of the cellular NN. However, most of the hardware models contain the inductor in circuit architecture [END 78, KIT 01, YAM 99, YAM 03]. If the system contains the inductor on the circuit system, it is difficult to implement the system to a complementary metal-oxide semiconductor integrated circuit (CMOS IC) chip.

We are researching the implementation of the hardware NN for a robot controlling system using HNMs [MAT 02, SAE 03, SAS 05, NAK 04, HAT 06, KEN 12a, KEN 12b]. The P-HNM has the same basic features of biological neurons, such as threshold, refractory period and spatiotemporal summation characteristics, and enables the generation of continuous action potentials. Furthermore, the P-HNM can oscillate without an inductor, therefore it is easy to implement the system to a CMOS IC chip [MAT 02, SAE 03]. Previously, we proposed the coupled neural oscillators using the P-HNMs. It was constructed by cell body models and synaptic models which have excitatory and inhibitory synaptic connections. We described the oscillating phenomena in an autonomous system [NAK 04, HAT 06]. This chapter presents the P-HNN which could output the PWM waveform of the PWM servo motor for robots.

In this chapter, first, we will show the examples of pulse specifications of the PWM servo motor. Second, we discuss the circuit diagram of the P-HNM and its basic characteristics. Third, we construct a P-HNN, and finally we will show results of the PWM servo motor control by the P-HNN.

5.2. PWM servo motor

Many robots used the PWM servo motor as an actuator to locomote the robot system. The PWM servo motor could be easily controlled by the programmed control by microcontroller. However, in the case of a more advanced robot controlling system compared with microcontroller controlling system, the robot system carries a computer controlling system or is wired by

cable to the computer controlling system [KAZ 98]. Consequently, advanced robot control by a compact system is desired. This section describes the examples of the PWM servo motor.

Figure 5.1 shows the example of pulse waveform to actuate the PWM servo motor. It is necessary to output the pulse waveform to control the servo motor. For example, we used the HRS-8498HB by Hitec Multiplex Japan for the PWM servo motor. Pulse specifications of a servo motor are shown in Table 5.1. These specifications are the measured control signal using an oscilloscope. It is shown that if the P-HNN can output the waveform such as shown in Figure 5.1 and satisfy the specifications of Table 5.1, the PWM servo motor could be controlled.

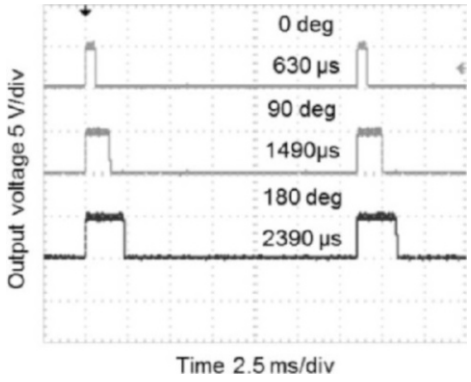

Figure 5.1. *Pulse waveform to actuate the servo motor*

Hitec Multiplex Japan HSR-8498HB	
Pulse period	16,040 µs
Peak-to-peak voltage	5.04 V
Motion range	0–180°
Increase of pulse width per degree	10 µs
Minimum pulse width (0°)	600 µs
Maximum pulse width (180°)	2,400 µs

Table 5.1. *Pulse specifications of servo motor*

5.3. Pulse-type hardware neuron model

The P-HNMs are used for the basic elements of the P-HNN. The P-HNM consists of a synaptic model, cell body model and axon model. In this section, we will show the circuit diagrams and consider the basic characteristics of the P-HNMs. The simulation results were given by OrCAD.

5.3.1. *Basic cell body model*

Figure 5.2 shows the circuit diagram of the basic cell body model. The cell body model consists of a voltage control type negative resistance circuit, an equivalent inductance circuit, and a membrane capacitor C_M and leak resister R_M. The voltage control type negative resistance circuit with equivalent inductance circuit consists of n-channel enhancement metal-oxide semiconductor field-effect transistor (MOSFET), p-channel enhancement MOSFET, voltage source V_A, resistor R_G and capacitor C_G. The cell body model has the negative resistance property that changes with time like a biological neuron, and enables the generation of a continuous action potential $v_M(t)$ by a self-excited oscillation and a separately excited oscillation. Moreover, the cell body model can switch between both oscillations by changing V_A. The separately excited oscillation occurs due to pulse train stimulus. In other word, the cell body model is an oscillator that has a voltage control type negative resistance circuit.

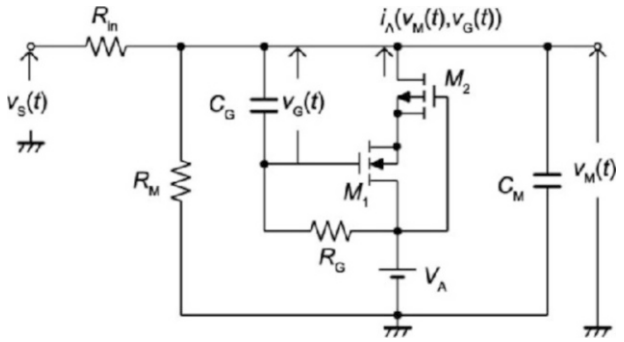

Figure 5.2. *Circuit diagram of basic cell body model*

The cell body model outputs the output voltage $v_M(t)$ in the case of inputting the input voltage $v_S(t)$, where $v_M(t)$ is the voltage at the end of capacitor C_M. $i_\Lambda(v_M(t), v_G(t))$ shows the nonlinear current, which flows in the

negative resistance circuit for output voltage, where $v_G(t)$ is the voltage at the end of capacitor C_G. Output voltage $v_M(t)$ and $v_G(t)$ were oscillatory waveforms which can be described by following simultaneous differential equations:

$$C_M \frac{dv_M(t)}{dt} = \frac{v_S(t)}{R_{in}} - \frac{v_M(t)}{R_M} - \frac{v_M(t) - v_G(t) - V_A}{R_G} + i_\Lambda(v_M(t), v_G(t)) \quad [5.1]$$

$$C_G \frac{dv_G(t)}{dt} = \frac{v_M(t) - v_G(t) - V_A}{R_G} \quad [5.2]$$

Nonlinear function $i_\Lambda(v_M(t), v_G(t))$ is shown as follows:

In the case of $v_G(t) + V_A + V_{Tn} + V_{Tp} < v_M(t) \le V_A + V_{Tp}$,

$$i_\Lambda(v_M(t), v_G(t)) = \frac{\beta}{8}(A+B)^2 \quad [5.3]$$

In the case of $V_A + V_{Tp} < v_M(t) \le v_G(t) + V_A + V_{Tn}$,

$$i_\Lambda(v_M(t), v_G(t)) = \frac{\beta(A)^2(A-2B)^2}{8(A+B)^2} \quad [5.4]$$

In the case of $v_G(t) + V_A + V_{Tn} < v_M(t) \le V_A$,

$$i_\Lambda(v_M(t), v_G(t)) = \left\{(V_A - v_M(t))(V_A - v_M(t) + 2A)(V_A + v_M(t) - 2V_{Tp})(V_A - 3v_M(t) + 2V_{Tp} + 2A)\right\} / 8(A+B)^2 \quad [5.5]$$

where $A = v_G(t) + V_{Tn}$, $B = V_{Tp} - v_M(t)$, V_{Tn} and V_{Tp} are threshold voltages of n- and p-channel MOSFETs, and k_n and k_p are conductance constants of n- and p-channel MOSFETs, respectively. In addition, we approximate the k_n and k_p as follows:

$$k_n = k_p = \frac{\mu\varepsilon}{2t}\frac{W}{L} = \frac{\beta}{2} \quad [5.6]$$

where μ is the carrier mobility, ε is the dielectric constant of gate oxide, t is the oxide film thickness, W is the channel width and L is the channel length.

Figure 5.3 shows an example of the phase plane of the circuit in Figure 5.2. The circuit parameters are β= 0.23 mA/V^2, V_{Tn} = 0.8 V, V_{Tp} = 1.5 V, C_M = 10 pF, C_G = 20 pF, R_M = 10 kΩ, R_G = 300 kΩ and V_A = 3.3 V. The abscissa is $v_M(t)$ and the ordinate is $v_G(t)$. The dotted line is $v_M(t)$-nullcline, the broken line is $v_G(t)$-nullcline and the solid line is the attractor, as shown in Figure 5.3. The attractor is drawn in a limit cycle. Moreover, Figure 5.3 shows that the cell body model has a characteristic of the class II neuron such as the Hodgkin–Huxley model or the Bonhoeffer–van der Pol model. In this chapter, we use the cell body model as a basic element of the coupled neural oscillator.

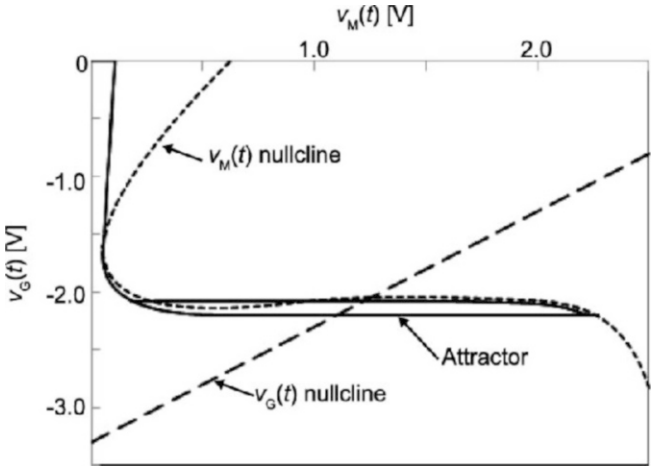

Figure 5.3. *Phase plane of basic cell body model*

5.3.2. *Cell body model for PWM controlling system*

The cell body model shown in Figure 5.2 is for CMOS IC circuit. The cell body model shown in Figure 5.4 is for a discrete circuit. Hereafter, the basic cell body model indicates the Figure 5.2 circuit and the cell body model indicates the Figure 5.4 circuit. In these circuits, we use BSS83 (©Koninklijke Philips Electronics N.V.) as an n-channel enhancement MOSFET M_{C1} and BSH205 (©Koninklijke Philips Electronics N.V.) as a

p-channel enhancement MOSFET M_{C2}. We add the bias circuit to the gate terminal of M_{C2}. The basic characteristics of Figure 5.4 and Figure 5.2 are equivalent. The circuit parameters are C_{CM} = 2.2 nF, C_{CG} = 1.2 nF, R_{CM} = 10 kΩ, R_{CG} = 390 kΩ, R_{Ca} = 20 kΩ, R_{Cb} = 15 kΩ and V_A = 3.3 V.

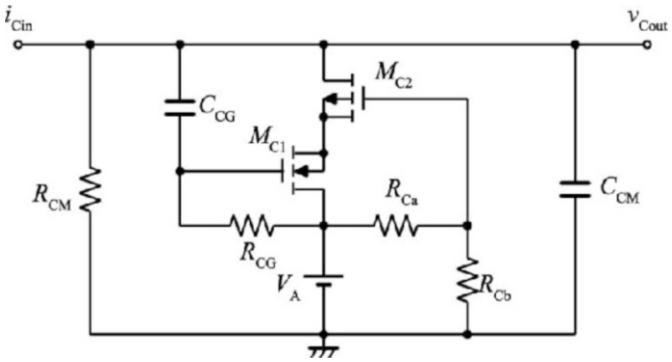

Figure 5.4. *Circuit diagram of cell body model for PWM controlling system*

Figure 5.5 shows the oscillatory characteristic of the Figure 5.4 circuit. This figure shows a cell body model that could oscillate in $3.4 \leq V_A \leq 4.7$ by self-excited oscillation. In this chapter, we set the cell body model to separately excited oscillation mode. Therefore, we set as V_A = 3.3 V.

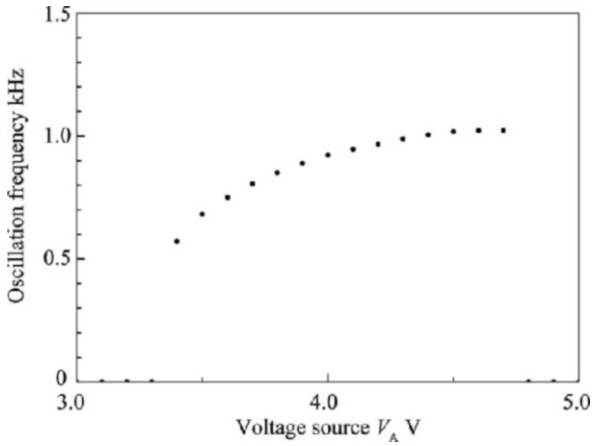

Figure 5.5. *Oscillatory characteristic of cell body model*

5.3.3. *Synaptic model*

Figure 5.6 shows the circuit diagram of a synaptic model. The synaptic model has the spatiotemporal summation characteristics similar to those of living organisms. The synaptic model spatiotemporal summated the outputs of cell body models according to synaptic weights. Synaptic weights are controlled by the synaptic weight control voltage V_{SC}. The circuit parameters of synaptic model are as follows: C_S = 1 pF; M_{S1}:W/L = 3; M_{S2}, M_{S3}, M_{S7}, M_{S8}:W/L = 1; M_{S4}:W/L = 0.25; M_{S5}:W/L = 5; and M_{S6}:W/L = 0.2. The voltage source is V_{DD} = 5 V.

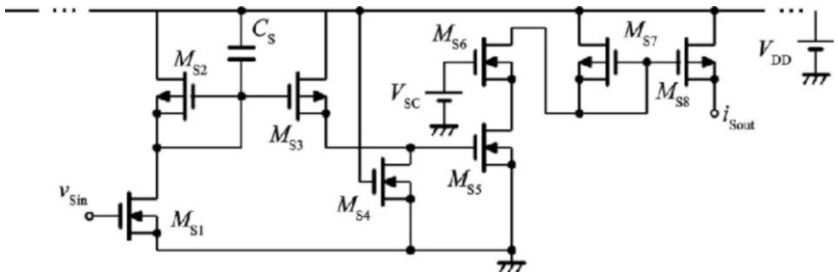

Figure 5.6. *Circuit diagram of synaptic model*

Figure 5.7 shows an example of output current i_{Sout} of the synaptic model in the case of a varying synaptic weight control voltage V_{SC}. This figure shows that the i_{Sout} could change by varying V_{SC}.

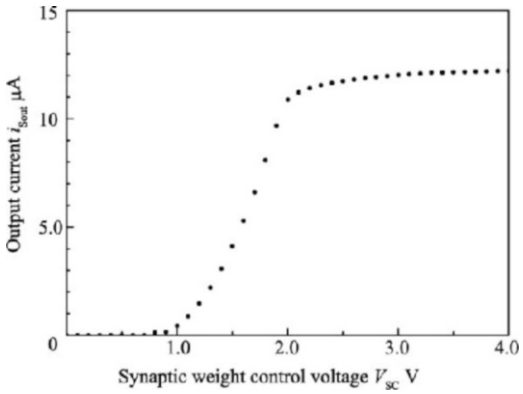

Figure 5.7. *Output current characteristic of synaptic model varying synaptic weight control voltage*

5.3.4. *Axon model*

Figure 5.8 shows the circuit diagram of an axon model. The axon models are a connected cascade. The axon model is an actively by distributed constant line which has the threshold function and waveform shaping function, just like living organisms. The input current of the axon model is i_{Ain}. The circuit parameters of the axon model are as follows: $C_{\mathrm{M}m}$ = 3.9 nF, $C_{\mathrm{G}m}$ = 1.5 nF, $R_{\mathrm{M}m}$ = 10 kΩ, $R_{\mathrm{G}m}$ = 390 kΩ, R_{am} = 20 kΩ and R_{bm} = 15 kΩ. The voltage sources are V_{A} = 3.3 V and V_{DD} = 5 V.

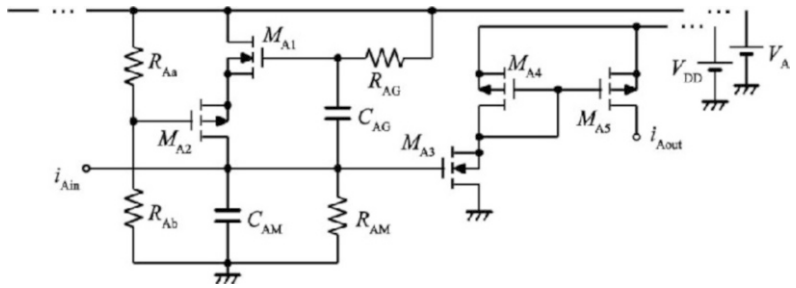

Figure 5.8. *Circuit diagram of axon model*

5.4. Pulse-type hardware neural networks

Figure 5.9 shows the schematic diagram of P-HNN. The P-HNN consists of cell body models, synaptic models and axon models. In the figure, *C* indicates a cell body model, A indicates an axon model and S indicates a synaptic model. The P-HNN consists of 24 cell body models, 25 synaptic models and 40 axon models. In the case of inputting the external trigger pulse to C_1, the pulse propagates the ring NN with delay time. One cell body model generates a pulse width of approximately 200 μs. Delay time of pulses is controled by the synaptic weights of S_n. By varying the synaptic weights, the PWM waveform width could change from 600 μs to 2,400 μs. However, the total length of the P-HNN will change with varying synaptic weights. Therefore, C_1' and S_1' will adjust the total length of the output waveform. In the case of increasing the synaptic weights of S_n, the synaptic weights of S_n' will decrease.

In the following, we will consider the basic characteristics of the P-HNN.

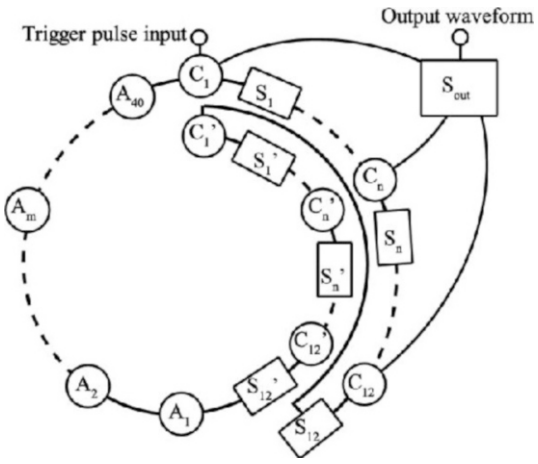

Figure 5.9. *Schematic diagram of the P-HNN*

Figure 5.10 shows the delay mechanism by varying the synaptic weights. In the case where synaptic weights are small, the input current of a cell body model is also small. Therefore, the pulse rise time will be longer. On the other hand, in the case where synaptic weights are large, the input current of a cell body model is also large. Thus, the pulse rise time will be shorter.

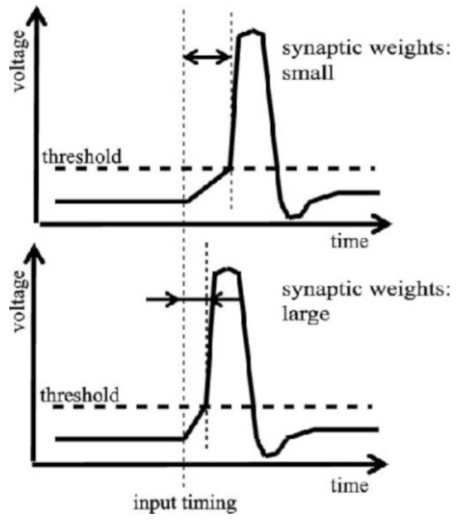

Figure 5.10. *Delay mechanism by varying the synaptic weights*

Figure 5.11 shows the delay time characteristic with varying synaptic weight control voltage V_{SC}. In the figure, the cell body model 1 (C_1) is connected to the cell body model 2 (C_2) by synaptic model (S_1). The delay time is the pulse interval between the output pulse of C_1 and C_2. It is shown that the delay time could change by varying the synaptic weights.

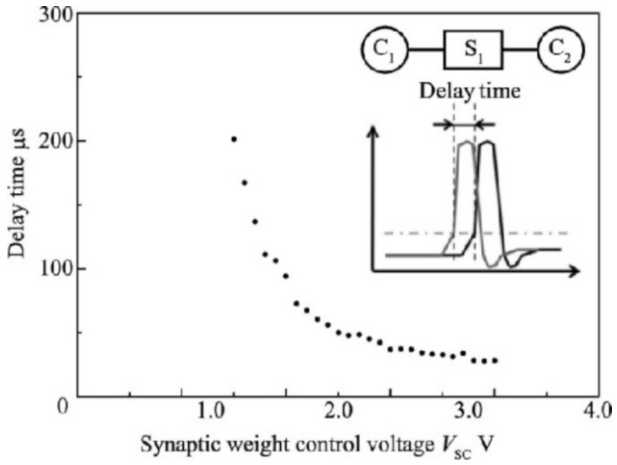

Figure 5.11. *Delay time characteristic with varying synaptic weight control voltage*

Figure 5.12 shows the mechanism for changing the pulse width of the PWM waveform. The pulses that have 200 μs pulse width are outputted by C_n ($1 \leq n \leq 12$). Therefore, changing the delay time by varying the synaptic weight could change the total length of 12 pulses. The synaptic model S_{out} of Figure 5.9 has added 12 pulses.

Figure 5.13 shows the pulse width of the PWM waveform and the angle of the PWM servo motor in the case of varying synaptic weight control voltage V_{SC}. In this figure, open circles indicate the pulse width and solid circles indicate the angle of the PWM servo motor. This figure shows that the P-HNN can change the pulse width of the output waveform by changing the synaptic weight control voltage.

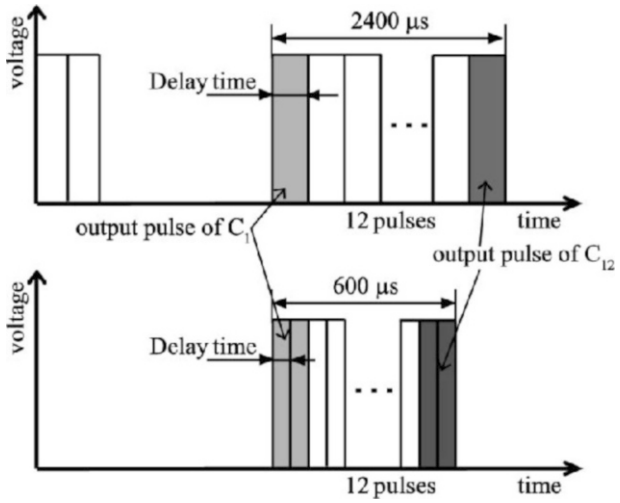

Figure 5.12. *Mechanism of changing the pulse width of the PWM waveform*

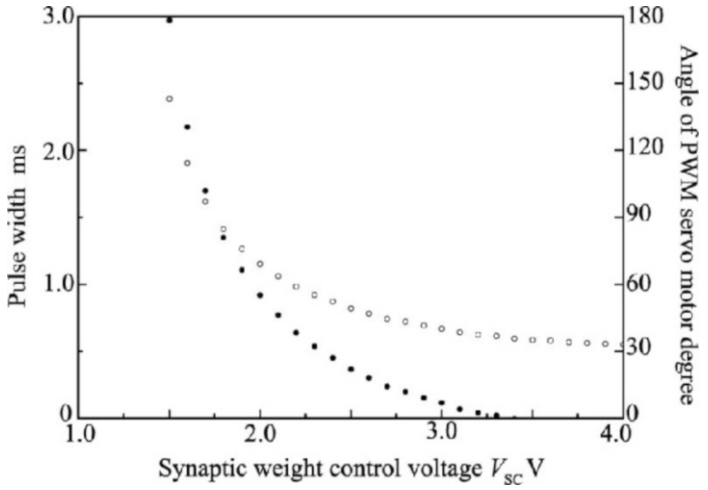

Figure 5.13. *Pulse width of the PWM waveform and angle of the PWM servo motor in the case of varying synaptic weight control voltage V_{SC}*

Figure 5.14 shows an example of the PWM waveform. It has been shown that the constructed P-HNN could output the PWM waveform by varying synaptic weight control voltage.

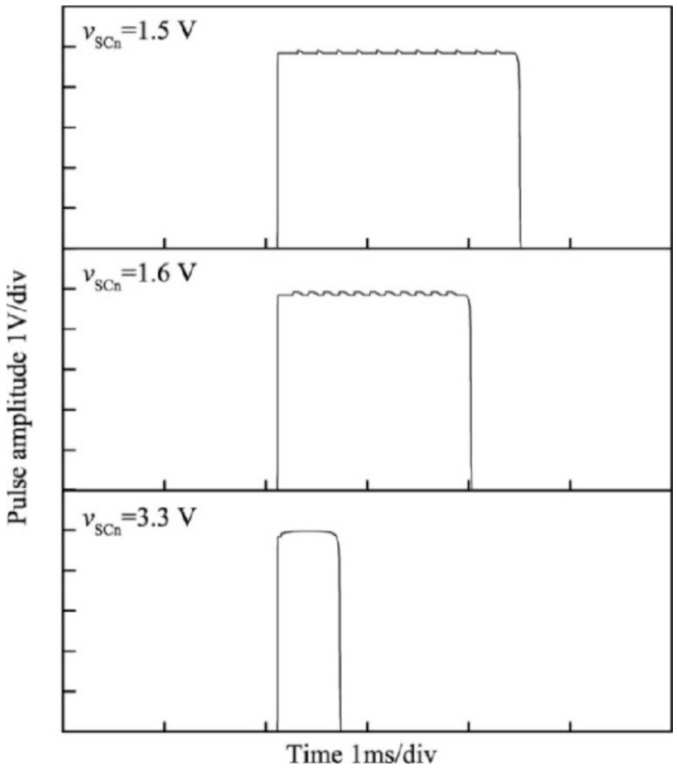

Figure 5.14. *Example of the generated PWM waveform*

5.5. Measurements of constructed discrete circuit

The measured results of the cell body model are shown in Figure 5.15. It is constructed by a discrete circuit. This figure shows that the pulse width of the constructed cell body model is longer than the designed value. Therefore, we have to adjust the parameters of the cell body model.

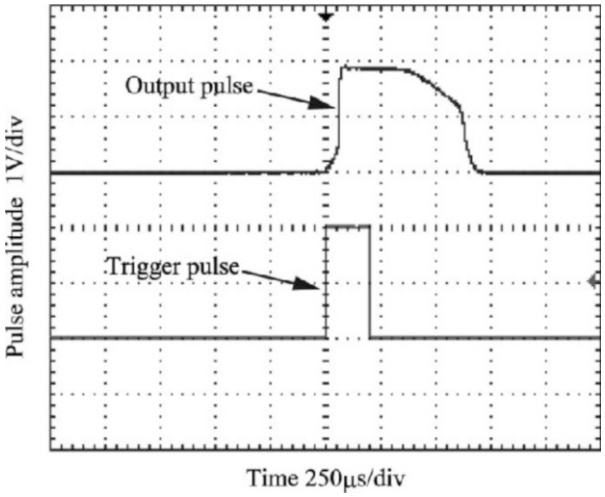

Figure 5.15. *Example of the output waveform of the P-HNM*

5.6. Conclusion

In this chapter, we presented the P-HNN which could output the PWM waveform of the PWM servo motor for robots. As a result, we generated the PWM waveforms of different pulse widths by varying the synaptic weights. The P-HNN realized the PWM servo motor control without using any software programs, or A/D converters. In addition, it is shown that the pulse waveform generation method of the P-HNM is same as for living organisms.

In the future, we will integrate the P-HNN circuit to the humanoid robot.

5.7. Acknowledgments

This research was supported by the JSPS KAKENHI (23760243), Nihon University College of Science and Technology Project Research, Nihon University Academic Research Grant (Total research, “11-002”). The fabrication of the silicon micro-robot was supported by the Research Center for Micro-Functional Devices, Nihon University.

5.8. Bibliography

[DEL 80] DELCOMYN F., "Neural basis of rhythmic behavior in animals", *Science*, vol. 210, pp. 492–498, 1980.

[END 78] ENDO T., MORI S., "Mode analysis of a ring of a large number of mutually coupled van del Pol oscillators", *IEEE Transactions on Circuits Systems*, vol. 25, no. 1, pp. 7–18, 1978.

[GEN 95] GENTARO T., "A model of the neuro-musculo-skeletal system for human locomotion", *Biological Cybernetics*, vol. 73, no. 2, pp. 97–111, 1995.

[GIS 01] GISZTER S., MOXON K., RYBAK I., *et al.*, "Neurobiological and neurorobotic approaches to control architectures for a humanoid motor system", *Robotics and Autonomous Systems*, vol. 37, no. 2, pp. 219–235, 2001.

[HAB 06] HABIB M.K., "Mechatronics engineering the evolution, the needs and the challenges", *Proceedings of the 32nd Annual Conference of IEEE Industrial Electronics Society* (IECON 2006), *IEEE*, pp. 4510–4515, 2006.

[HAB 07] HABIB M.K., "Real time mapping and dynamic navigation for mobile robots", *International Journal of Advanced Robotic Systems*, vol. 4, no. 3, pp. 323–338, 2007.

[HAB 08] HABIB M.K., "Interdisciplinary mechatronics: problem solving, creative thinking and concurrent design synergy", *International Journal of Mechatronics and Manufacturing Systems* (*IJMMS*), vol. 1, no. 1, pp. 264–269, 2008.

[HAT 06] HATA K., SAEKI K., SEKINE Y., "A pulse-type hardware CPG model for quadruped locomotion pattern", *International Congress Series*, vol. 1291, March, pp. 157–160, 2006.

[JIA 02] JIANG S., FUMIO N., "Neural locomotion controller design and implementation for humanoid robot HOAP-1", *Proceedings of the 20th Annual Conference of the Robotics Society of Japan*, Osaka, Japan, 12–14 October 2002.

[KAZ 98] KAZUO H., MASATO H., YUJI H., *et al.*, "The development of Honda humanoid robot", *Proceedings of the 1998 IEEE International Conference on Robotics & Automation*, Leuven, Belgium, pp. 1321–1326, May 1998.

[KEN 12a] KEN S., AKIHIRO M., KATSUTOSHI S., *et al.*, "Synchronization of coupled pulse-type hardware neuron models for CPG model", *The Relevance of the Time Domain to Neural Network Models, Springer Series in Cognitive and Neural Systems*, vol. 3, pp. 117–133, 2012.

[KEN 12b] KEN S., MINAMI T., YOSHIFUMI S., *et al.*, "Synchronization of coupled pulse-type hardware neuron models for CPG model", *International Journal of Advanced Robotic Systems*, vol. 9, no. 226, pp. 1–6, 2012.

[KIT 01] KITAJIMA H., YOSHINAGA T., AIHARA K., *et al.*, "Burst firing and bifurcation in chaotic neural networks with ring structure", *International Journal of Bifurcation and Chaos*, vol. 11, no. 6, pp. 1631–1643, 2001.

[KIY 87] KIYOTOSHI M., "Mechanisms of frequency and pattern control in the neural rhythm generators", *Biological Cybernetics*, vol. 56, nos. 5–6, pp. 345–353, 1987.

[KUN 03] KUNICHIKA T., TETSUYA Y., KAZUYUKI A., *et al.*, "Bifurcations in synaptically coupled Hodgkin-Huxley neurons with a periodic input", *International Journal of Bifurcation and Chaos*, vol. 13, no. 3, pp. 653–666, 2003.

[KUN 06] KUNICHIKA T., TETSUYA Y., HITOSHI I., *et al.*, "Bifurcations in a mathematical model for circadian oscillations of clock genes", *Journal of Theoretical Biology*, vol. 239, no. 1, pp. 101–122, 2006.

[MAT 02] MATSUOKA J., SEKINE Y., SAEKI K., *et al.*, "Analog hardware implementation of a mathematical model of an asynchronous chaotic neuron", *IEICE Transactions on Fundamentals*, vol. E85-A, no. 2, pp. 216-221, February 2002.

[MIC 02] MICHAEL A., *The Handbook of Brain Theory and Neural Networks*, 2nd ed., MIT Press, Cambridge, MA, 2002.

[NAK 04] NAKABORA Y., SAEKI K., SEKINE Y., "Synchronization of coupled oscillators using pulse-type hardware neuron models with mutual coupling", *Proceedings of the 2004 International Technical Conference on Circuits/Systems, Computers and Communications* (ITC-CSCC 2004), pp. 8D2L-3-1–8D2L-3-4, 2004.

[NAO 01] NAOMICHI O., NOBUTOSHI Y., "Generation of human bipedal locomotion by a bio-mimetic neuro-musculo-skeletal model", *Biological Cybernetics*, vol. 84, no. 1, pp. 1–11, 2001.

[RIA 02] RIADH Z., FUMIO N., "Recurrent neural network language for robot learning", *Proceedings of the 20th Annual Conference of the Robotics Society of Japan*, Osaka, Japan, 12–14 October 2002.

[SAE 03] SAEKI K., SEKINE Y., "CMOS implementation of neuron models for an artificial auditory neural network" *IEICE Transactions on Fundamentals*, vol. E86-A, no. 2, pp. 248–251, February 2003.

[SAS 05] SASANO N., SAEKI K., SEKINE Y., "Short-term memory circuit using hardware ring neural networks", *Artificial Life and Robotics*, vol. 9, no. 2, pp. 81–85, June 2005.

[SHI 07] SHIGEKI T., TETSUSHI U., HIROSHI K., *et al.*, "Bifurcation analysis of current coupled BVP oscillators", *International Journal of Bifurcation and Chaos*, vol. 17, no. 3, pp. 837–850, 2007.

[SIM 00] SIMON F., KAREN A., ILYA R., *et al.*, "A neurobiological perspective on humanoid robot design", *IEEE Intelligent Systems*, vol. 15, no. 4, pp. 64–69, 2000.

[YAM 99] YAMAUCHI M., WADA M., NISHINO Y., *et al.*, "Wave propagation phenomena of phase states in oscillators coupled by inductors as a ladder", *IEICE Transactions on Fundamentals*, vol. E82-A, no. 11, pp. 2592–2598, November 1999.

[YAM 03] YAMAUCHI M., OKUDA M., NISHINO Y., *et al.*, "Analysis of phase-inversion waves in coupled oscillators synchronizing at in-and-anti-phase," *IEICE Transactions on Fundamentals*, vol. E86-A, no. 7, pp. 1799–1806, July 2003.